Test of microscopic optical model potentials for neutron elastic scattering at 14.6 MeV over a wide mass range

L. F. Hansen, F. S. Dietrich, B. A. Pohl, C. H. Poppe, and C. Wong
Lawrence Livermore National Laboratory, University of California, Livermore, California 94550
(Received 27 August 1984)

Differential cross sections for the elastic scattering of 14.6 MeV neutrons from ^{9}Be, C, ^{27}Al, Fe, ^{59}Co, ^{89}Y, ^{93}Nb, In, ^{140}Ce, ^{181}Ta, ^{197}Au, ^{208}Pb, and ^{209}Bi have been measured using a time-of-flight facility. The measured cross sections cover the angular range from 9.2° to 159°. Calculations have been carried out using two local microscopic optical potentials, based on the work of Jeukenne, Lejeune, and Mahaux, and of Brieva and Rook. Reasonably good agreement with the measurements is found over the whole mass range, with the Jeukenne-Lejeune-Mahaux potential giving systematically better agreement with the data. The quality of the results with the Jeukenne-Lejeune-Mahaux potential compares well with that obtained from phenomenological optical model calculations using global parameters.

I. INTRODUCTION

A large number of neutron elastic differential cross section measurements at 14—15 MeV have appeared in the literature[1−36] in the last 30 years on targets ranging from hydrogen to uranium. The measurements and analyses have been carried out under quite different conditions, which include beam energy resolution, size and geometry of the targets, flight paths, detector efficiency, and techniques to correct for effects due to the large targets. As a result, wide variations are observed in the quality of the data. Typically, the data have been fit by a phenomenological optical-model analysis. Global optical model (OM) parameter sets, such as those of Bjorklund and Fernbach,[37] Perey and Buck,[38] Wilmore and Hodgson,[39] Becchetti and Greenlees,[40] and Rapaport *et al.*,[41] have been used. Improved fits for individual nuclei have been obtained with parameters that vary somewhat from those of the global sets. This work reports measurements at 14.6 MeV from ^{9}Be, C, ^{27}Al, Fe, ^{59}Co, ^{89}Y, ^{93}Nb, In, ^{140}Ce, ^{181}Ta, ^{197}Au, ^{208}Pb, and ^{209}Bi. The purpose of these measurements was to provide a consistent data set for further optical-model analyses. The new data set has been analyzed using two different microscopic optical potentials,[42−45] and has also been compared with the predictions of the global optical potential of Rapaport *et al.*[41]

In recent years, two local microscopic optical potentials, due to Jeukenne, Lejeune, and Mahaux (JLM),[42,43] and Brieva and Rook,[44,45] have been shown[44−47,57,58] to give reasonable agreement between calculations of elastic scattering differential cross sections and proton and neutron scattering measurements. These potentials are based on a free nucleon-nucleon potential, and the scattering in nuclear matter is calculated by solving the Bethe-Goldstone equation. The two approaches differ in the choice of the free nucleon-nucleon potential, the techniques used in many-body calculations, and the way in which a local-density approximation is applied to relate the optical potential in finite nuclei to the results of nuclear matter calculations. The JLM approach begins with the Reid hard-core potential and computes the complex optical potential in nuclear matter as a function of energy and density. On the other hand, the Brieva-Rook approach is based on the Hamada-Johnston potential and yields a local, complex, energy and density dependent effective interaction that approximates the nuclear matter g matrix; this effective interaction is folded with the nuclear density to yield the optical potential.

The analysis of the present measurements is part of a program to test systematically these two microscopic models for both proton and neutron scattering over a wide range of masses and energies,[48,49] using a consistent set of approximations and calculational techniques. In the present work we discuss the comparison of the microscopic calculations with our recent measurements of the neutron elastic differential cross sections at 14.6 MeV for 13 targets between Be and Bi which are either separated isotopes or natural samples that are nearly isotopically pure. This comparison would have been much less effective with only the existing 14 MeV data,[1−36] given the heterogeneity in the experimental conditions and the lack of isotopically-pure targets in the mass range $9 \leq A \leq 209$.

In addition to the comparisons with the microscopic potentials, the data have been compared with calculations carried out with phenomenological optical model potentials for two global parameter sets, the Becchetti-Greenlees,[40] and the Rapaport *et al.*[41] global potentials. The results obtained with these two sets[40,41] are quite similar, with Rapaport *et al.* (the "Ohio set") giving slightly better agreement with the measurements. The parameters in the Ohio set have been obtained from an analysis of neutron elastic scattering measurements from Ca to Pb in the energy range 7—26 MeV.

II. EXPERIMENTAL APPARATUS AND PROCEDURE

The measurements have been made using as a 14.6 MeV neutron source the ^{2}H(d,n)^{3}He reaction at 0° with a 12

MeV incident deuteron beam from the Lawrence Livermore National Laboratory (LLNL) tandem electrostatic accelerator. The beam was bunched, 1—2 ns wide, and swept at a 2.5 MHz burst rate. The deuterium target was a 1 cm diameter by 3 cm long gas cell filled to a pressure of 2 atm. The cell, a stainless steel cylinder with a 0.038 cm wall thickness, had a 5.26 mg/cm^2 Havar entrance window and a 984 mg/cm^2 Au stop, and was mounted at the end of a 30 cm long, low mass, stainless steel stem. Two identical cells mounted on their respective parallel stems which could rotate into position in the deuterium beam path were used during the measurements. One cell was filled to 2 atm of deuterium gas and the second one was evacuated in order to measure the neutron background contribution from the empty cell.

The zero degree 14.6 MeV neutron burst impinged on the scattering samples positioned at 20 cm from the gas cell. The targets, Be, C, Al, Fe, Co, Y, Nb, In, ^{140}Ce, Ta, Au, ^{208}Pb, and Bi, were nominally cylinders of 2.5 cm diameter and 5 cm height. They were mounted on a hollow, 1 cm diameter nylon pole whose contribution to the background was negligible because of its very small mass.

The scattered neutrons were detected using the LLNL time-of-flight (TOF) facility[50] in which 16 NE213 liquid scintillator detectors (11.3 cm diameter by 5.1 cm long) allow simultaneous measurements in the angular region from 3.5° to 159° (see Fig. 1). In the present work the elastic differential cross sections were measured between 9.2° and 159° and the flight path was 10.75 m for all the detectors. The neutron detector bias was 5.4 MeV, and pulse-shape discrimination was used to reduce the gamma-ray background.

The efficiency of the NE213 detectors was calculated with the Livermore code EFFIC; this efficiency, when used to analyze the measurement of the differential cross sections for the ^{2}H(d,n)^{3}He neutron source reaction using the 16 detectors, reproduces well Drosg's[51] evaluation of the angular distribution for this reaction. A small stilbene detector, 5.08 cm diameter by 5.08 cm thick, positioned in a shielded enclosure at ~40° and 10 m from the target, was used as a neutron flux monitor.

In order to carry out the present measurements, additional shielding was installed in the TOF facility to improve the ratio of the neutrons scattered from the target to those coming directly from the gas cell. Figure 1 shows a schematic view of the shielding arrangement installed close to the gas cell-target system. It is composed of a set of 16 wedges distributed in angle around the target at a radius of 30 cm, covering the angular range 9.2°—159°. Each wedge, 5.04 cm thick and 1 m long, has two sections; the 30 cm closest to the target is lead and the remaining 70 cm is iron. This shielding resulted in ratios of scattered-to-transmitted neutrons that were improved by factors of 20 to 50 over the values obtained without the wedges for the fifteen detectors.

III. EXPERIMENTAL RESULTS

To account for the different sources of background, four spectra were measured for each target: *A*, sample in/gas in; *B*, sample out/gas in; *C*, sample in/gas out; and *D*, sample out/gas out. The net counts (NC) from the scatterer alone are given by

$$\mathrm{NC}=[(\text{sample in})-K_1(\text{sample out})]_{\text{gas in}}-K_3[(\text{sample in})-K_2(\text{sample out})]_{\text{gas out}}\ , \tag{1}$$

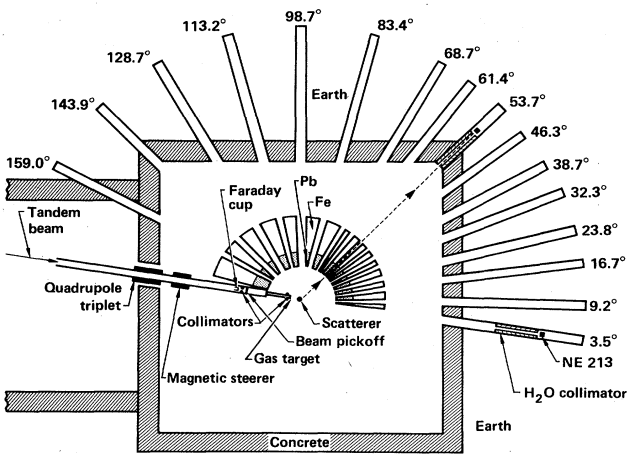

FIG. 1. Schematic representation of the Livermore time-of-flight facility and wedge shielding used in the present measurements. The 3.5° detector, turned off for an elastic scattering run, is used to measure the incident flux on the scatterer per monitor count (see the text).

where K_1, K_2, and K_3 are normalization constants, with K_1 normalized to the monitor and K_2 and K_3 normalized to charge. For K_1, the monitor and charge normalization agree within statistical uncertainties.

The detector and monitor counts were corrected for dead time, which was larger for the "gas in" spectra, but always less than 5%. Figure 2 shows a comparison of the four spectra *A*, *B*, *C*, and *D* for carbon at 9.2 deg. The contributions to the background from the empty cell are rather small and can be neglected for the elastic peaks at forward angles; however, it is important to subtract them at the minima of the elastic angular distributions and for inelastic differential cross sections. The net counts due to elastic scattering were obtained from Gaussian fits to the peaks in the net spectra given by Eq. (1), assuming the background to be linear. Multiple scattering corrections, flux attenuation in the scattering sample, and finite angular resolution corrections were calculated with the Monte Carlo code MULCAT.[52]

The uncertainties in the relative differential cross sections are about 6% for the forward angles, increasing to approximately 15—20 % for some of the backward angles and smaller targets (e.g., Au: 1 cm diameter, 2 cm height).

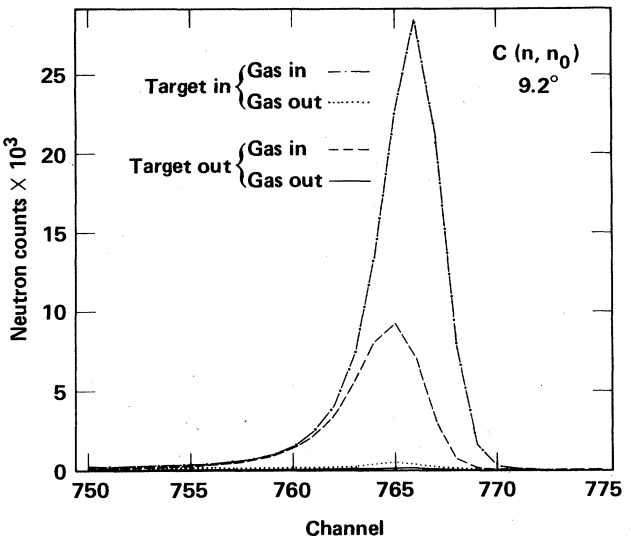

FIG. 2. Neutron elastic peak at 9.2° from the C target bombarded with 14.6 MeV neutrons. The curves correspond to the four measurements carried out to account for all sources of background contributions (see the text).

These uncertainties include the statistical counting error and the error (~5%) in the shape of the detector efficiency versus energy curve. In addition, there is an uncertainty in the absolute differential cross sections which arises from the uncertainty in determining the incident neutron flux per monitor count (~3%), and the error in measuring the distance between the gas cell and the target (1—2 %). In computing the statistical counting error on the differential elastic cross sections, it was assumed that the net spectra given by (1) were obtained in a direct measurement. Hence, the statistical error computation ignores the contributions from K_1, K_2, and K_3. This error agrees well with the exact value obtained by differentiating (1), since in the present measurements the constant K_1 is ~1, and the counts with the gas out are negligible such that the K_2 and K_3 terms in Eq. (1) are small effects in the calculation of the error. The absolute cross sections are obtained from measuring at 3.5° the neutron flux incident on the scatterer per monitor count. The error in the incident neutron flux per monitor count is determined mainly by the number of counts accumulated in the low count-rate monitor. The length of runs is such that the counts in the monitor have between 2—3 % statistical errors. Finally, the statistical errors in the Monte Carlo calculations of the target geometry corrections were less than 1%. The measured differential cross sections are shown in Figs. 3—8 together with the calculations to be discussed.

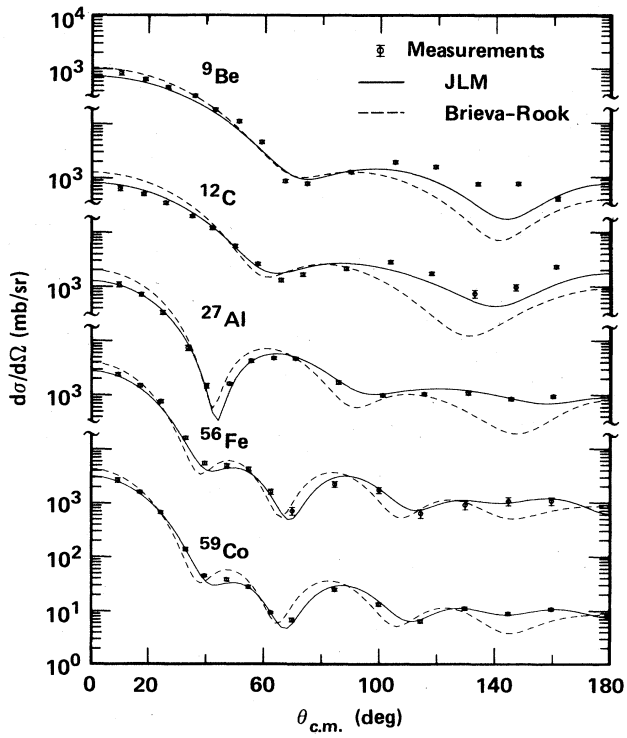

FIG. 3. Measurements of the neutron elastic differential cross sections for ^{9}Be, C, ^{12}Al, Fe, and ^{59}Co. Calculations carried out with the microscopic OMP of Jeukenne-Lejeune-Mahaux (JLM: solid lines) and that of Brieva-Rook (dashed lines). For C and Fe the calculations have been done assuming 100% ^{12}C and ^{56}Fe isotopic composition, respectively.

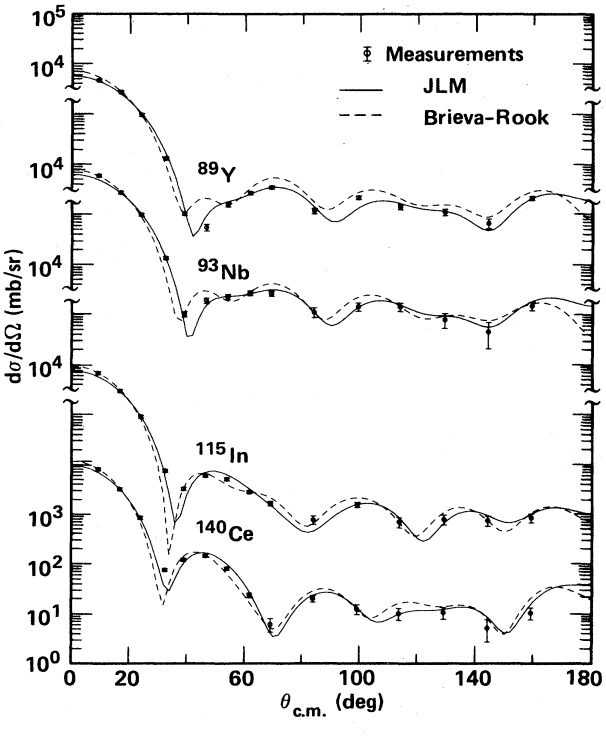

FIG. 4. Measurements of the neutron elastic differential cross sections for ^{89}Y, ^{93}Nb, In, and ^{140}Ce. Calculations carried out with the microscopic OMP of Jeukenne-Lejeune-Mahaux (JLM: solid lines) and that of Brieva-Rook (dashed lines). For In, the calculations have been done assuming 100% ^{115}In isotopic composition.

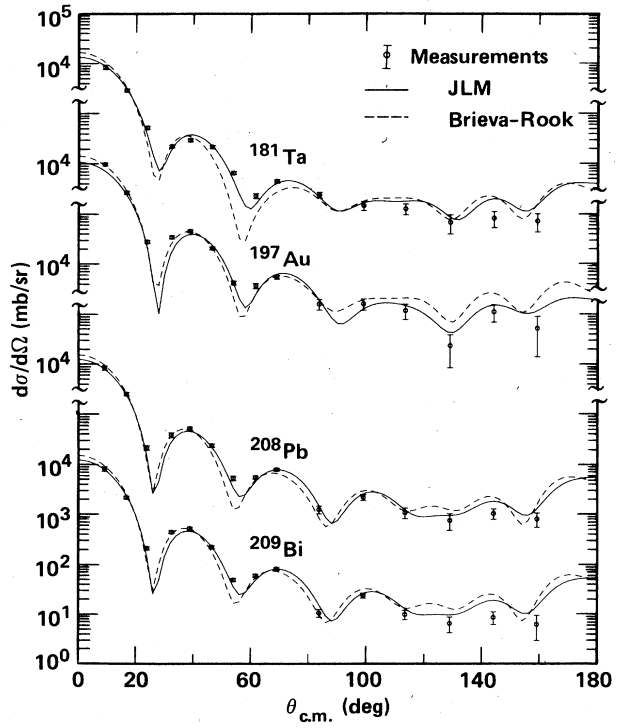

FIG. 5. Measurements of the neutron elastic differential cross sections for ^{181}Ta, ^{197}Au, ^{208}Pb, and ^{209}Bi. Calculations carried out with the microscopic OMP of Jeukenne-Lejeune-Mahaux (JLM: solid lines) and that of Brieva-Rook (dashed lines).

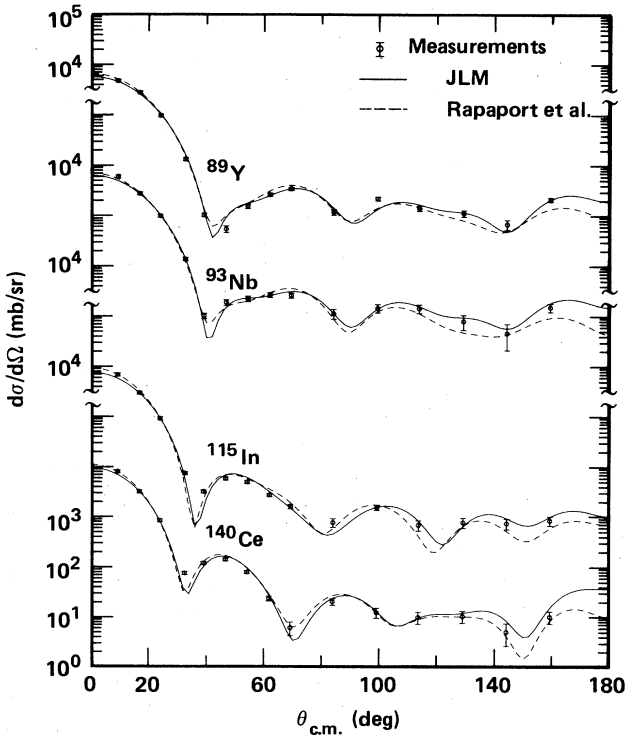

FIG. 7. Same as in Fig. 4 except dashed curves refer to calculations using the OMP of Rapaport *et al.*

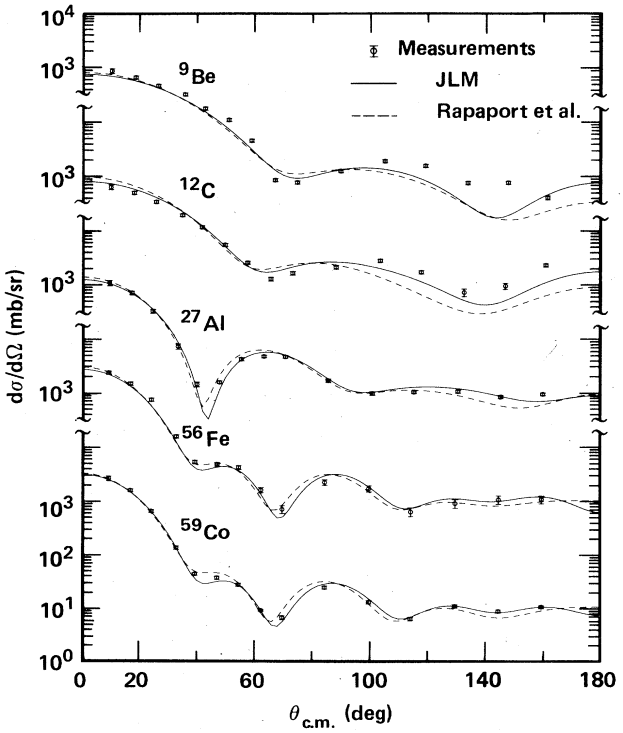

FIG. 6. Same as in Fig. 3 except dashed curves refer to calculations using the OMP of Rapaport *et al.*

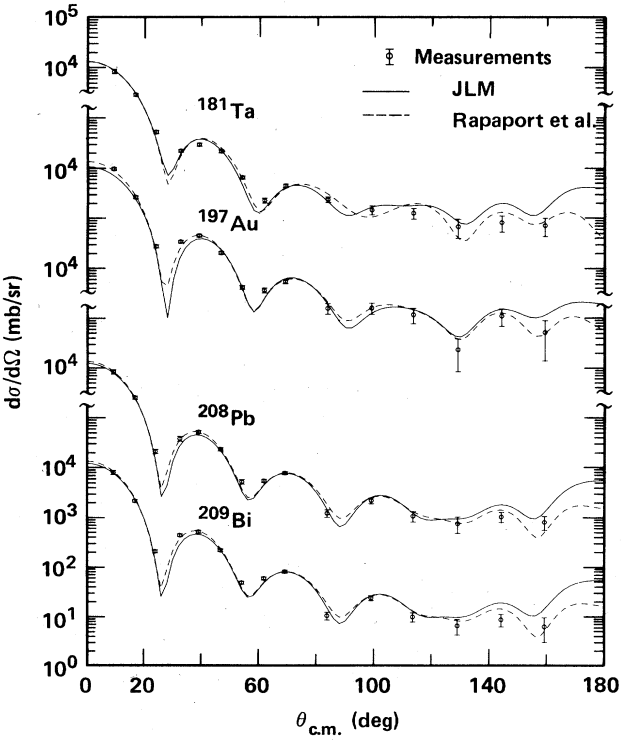

FIG. 8. Same as in Fig. 5 except dashed curves refer to calculations using the OMP of Rapaport *et al.*

IV. OPTICAL-MODEL ANALYSIS OF THE DATA

A. Microscopic calculations

The microscopic optical potentials were calculated by folding an effective interaction with the nuclear density; details of how this was done may be found in Ref. 49 for both the real and spin-orbit potentials. As in Ref. 49, only the central potential was calculated from the JLM and Brieva-Rook procedures. The effective interaction used to calculate the spin-orbit potential was taken from the work of Bertsch *et al.*[53] (Elliott matrix elements). The spin-orbit potential is real and independent of energy and density. The real and imaginary components of the central part of the optical potential were multiplied by normalizing constants λ_V and λ_W, respectively, and these parameters were adjusted by least squares for an optimal fit to the data. The values of these parameters are shown in Table I. No adjustment of the spin-orbit potential was made, as it appears to reproduce elastic analyzing power data below 25 MeV very well without alteration.[49]

Proton densities were taken from the results of electron scattering experiments.[54] In the light and medium weight nuclei (^{9}Be to ^{93}Nb) the neutron density was assumed proportional to the proton density, whereas a small increase in the neutron rms radius relative to that for protons (up to 2.6%) was used for a number of the heavier nuclei, as expected from Hartree-Fock and droplet-model calculations. Sample calculations made with different shapes for the neutron and proton densities did not yield results significantly different from those with the same shapes. This is as expected, since neutron scattering is very insensitive to these rather small differences between neutron and proton radii,[48] mainly because of the weakness of the neutron-neutron interaction relative to that between neutrons and protons in the present energy range.

An improvement was made in the treatment of the exchange term when using the Brieva-Rook interaction. In previous works[44,45,49] the self-consistent wave number used in making a local approximation to the nonlocal exchange term has been determined from the purely real expression

$$\hbar^2 k(r)^2/2m = E - \mathrm{Re}\ U(r)\ ,$$

where $\mathrm{Re}\,U(r)$ is the real part of the central optical potential. In the present work we have used the complex self-consistent wave number obtained by inserting the entire, complex central potential in the preceding equation. General treatments[55] of the Perey-Buck transformation show that the complex wave number is the appropriate approximation in reducing a nonlocal potential to an equivalent local one. The practical consequences of the improved approximation in the present energy range are an overall reduction of the volume integral of the imaginary potential by 15—20% relative to calculations with a real wave number, and a slight increase in the surface-to-volume ratio of the imaginary component, which is in the direction of improved consistency with phenomenological potentials. All of the Brieva-Rook calculations were performed with both prescriptions, although only those with the complex self-consistent wave number are presented here. The normalizing parameters, shown in Table I and Fig. 9, are larger by 15—20% than those obtained with the real wave number, but the observable quantities (angular distributions, total and reaction cross sections) are very similar with the two procedures after the normalization has been applied.

The comparison between the predictions of the microscopic models (after normalization) and the angular distribution data is shown in Figs. 3—5. The total cross sections predicted by the normalized potentials are shown in Table II, along with the measurements reported by Foster and Glasgow.[56]

Both microscopic approaches give reasonable results in view of the limited number of free parameters in the calculations. However, the JLM potentials yield systemati-

TABLE I. Values of χ^2/N and the normalization parameters λ_V and λ_W for the neutron elastic differential cross sections at 14.6 MeV, compared with the Brieva-Rook and JLM microscopic optical model potentials and with the Rapaport *et al.* set *A* global potential.

	Brieva-Rook			JLM			Rapaport *et al.*		
Target	χ^2/N	λ_V	λ_W	χ^2/N	λ_V	λ_W	χ^2/N	λ_V	λ_W
Be	46.4	0.94	1.23	29.4	1.00	1.25	40.2	0.96	0.83
C	60.3	1.03	1.59	14.1	1.04	1.04	32.5	0.96	0.67
Al	51.1	1.02	1.68	6.3	0.99	1.06	12.0	0.96	0.72
Fe	13.0	1.04	1.52	3.9	0.96	0.97	4.0	1.00	0.78
Co	32.8	1.02	1.48	2.6	0.95	0.96	6.7	0.98	0.82
Y	38.5	1.02	1.08	5.5	0.97	0.92	8.0	1.00	0.84
Nb	9.6	1.02	1.28	2.0	0.96	0.94	2.2	0.98	0.96
In	12.7	1.00	1.51	7.2	0.98	1.18	7.6	1.00	1.07
Ce	12.9	1.01	1.19	7.6	0.97	0.92	7.5	1.02	0.84
Ta	24.9	0.99	0.98	6.8	0.94	0.70	6.5	0.99	0.87
Au	7.4	1.00	1.00	7.6	0.98	1.00	3.1	0.99	0.92
Pb	11.0	1.01	0.97	4.0	0.97	0.81	2.9	1.00	0.84
Bi	17.6	1.01	0.92	8.2	0.97	0.80	6.4	1.00	0.82

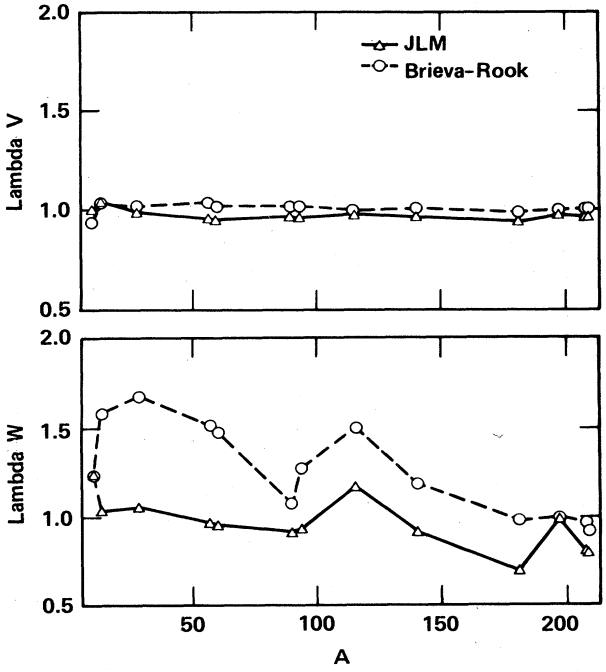

FIG. 9. Normalizing parameters λ_V and λ_W for the real (V) and imaginary (W) potentials, respectively, determined from a least square fit to measured elastic angular distributions. Triangles, Jeukenne-Lejeune-Mahaux OM potentials; circles, Brieva-Rook OM potentials. The solid and dashed lines have been drawn only to guide the eye.

cally better quantitative agreement with the data than the Brieva-Rook potentials, and the difference between the two sets of calculations becomes more pronounced with decreasing target mass. These differences appear mainly in the large angle ($>80°$) behavior of the angular distributions and in the tendency for the Brieva-Rook potentials to systematically overpredict the total cross sections, except in the heaviest nuclei.

The normalizing parameters λ_V for the real central potential are gratifying close to unity (within a few percent) in all cases, which indicates that the volume integrals are correctly predicted in both models. However, the shapes of the real potentials are strikingly different, with the Brieva-Rook potentials showing a strong deviation from a Woods-Saxon shape because of the presence of a "bump" in the region of the nuclear surface.[44,45,49] In a study[52] of the Brieva-Rook and JLM potentials for nucleon scattering on medium-mass nuclei (^{54,56}Fe), an examination of the behavior of the potentials in momentum space led to the conclusion that both the difficulties in reproducing the large-angle differential cross sections and the overestimate of the total cross sections with the Brieva-Rook potential were correlated with the unusual shape of the real potential. These results are consistent with the worsening agreement between calculation and experiment with decreasing mass in the present study, since the surface region where the unusual behavior occurs becomes a larger fraction of the nuclear volume as the target mass decreases. Indeed, such non-Woods-Saxon shapes are expected[57,58] in the medium-energy range (>100 MeV). However, on the basis of the present results and the earlier study of ^{54,56}Fe it appears that the surface bump is too pronounced in the lower energy range ($\lesssim 26$ MeV). It is not clear at the present time whether this anomaly is due to the use of the Hamada-Johnston interaction, which has an unusually hard core, or whether it reflects an inaccuracy in deriving the density dependence of the effective interaction.

The normalizing constants λ_W for the imaginary potential show more scatter than those for the real potential, but nevertheless a reasonably smooth trend with mass is evident for both the Brieva-Rook and JLM potentials. The parameter λ_W for the Brieva-Rook potentials shows a tendency to decrease with increasing target mass. The mass dependence of λ_W is less marked for the JLM potentials, although there is a suggestion of a slight decrease toward the higher masses for these potentials also. The

TABLE II. Values of the neutron total cross sections, σ_T, at 14.6 MeV calculated with the normalized Brieva-Rook and JLM microscopic OMP and the normalized Rapaport *et al.* (Ref. 41) global OMP. The experimental values are from Foster and Glasgow (Ref. 56). All cross sections are in barns.

Target	Brieva-Rook	JLM	Rapaport *et al.*	Experiment
Be	1.69	1.44	1.50	1.43
C	1.82	1.45	1.60	1.39
Al	2.19	1.73	1.83	1.78
Fe	3.03	2.52	2.65	2.47
Co	3.14	2.69	2.76	2.86
Y	4.07	3.62	3.89	3.79
Nb	4.21	3.77	3.97	3.84
In	4.62	4.14	4.58	4.43
^{140}Ce	5.14	4.64	4.99	4.84
Ta	6.15	5.51	5.40	5.40
Au	5.59	4.87	5.46	5.29
^{208}Pb	5.83	5.25	5.46	5.51
Bi	5.79	5.22	5.46	5.58

mean value and standard deviation of λ_W are 0.96 ± 0.15 for the JLM potentials; these quantities show that the magnitude of the imaginary potential is predicted rather accurately by the JLM approach. The shapes of the imaginary potentials differ from those of phenomenological potentials, which are usually surface peaked at this energy with little or no volume component. The JLM potential shows a pronounced surface peak, but there is also a significant volume component (3.7 MeV at the origin). The Brieva-Rook potential may be roughly described by a predominantly volume form with a small surface peak. These deviations from the phenomenological results may represent a deficiency of the local density approximation, since explicit finite-nucleus effects (such as the coupling of the probe to nuclear surface vibrations) are not accurately treated.

Both microscopic potentials underpredict the back-angle cross sections in the lightest nuclei (^{9}Be and ^{12}C). Apart from possible inaccuracies in the details of the present treatment and of the local density approximation when applied to light nuclei, this deficiency may indicate the necessity of adding exchange terms other than the single-nucleon knockout contributions that have been included in the present work. Such terms have been shown to affect the back-angle cross sections in very light nuclei.[59] For zero-spin targets, the problem is probably not due primarily to channel-coupling effects, since a coupled-channel treatment[60] of neutron scattering from ^{12}C with phenomenological potentials shows that the effect of channel coupling on elastic scattering is not very important after the potential strengths are readjusted. For nuclei of spin one and greater, on the other hand, a quadrupole deformation affects elastic scattering directly via a one-step process. Such an effect has been shown[61] in ^{7}Li to remedy a back-angle deficiency very much like that exhibited by ^{9}Be in the present work.

B. Phenomenological calculations

The quality of the fits obtained with the microscopic optical model potential (OMP) have been compared with calculations carried out with global[41] OM parameters optimized to fit neutron data in the 7–26 MeV energy range. The OM calculations were performed with the parameters given in Ref. 41 as set A for $E \leq 15$ MeV; however, the strengths of the central-potential terms were normalized in fitting the data, as described in the following. The values of the parameters before normalization, in a standard form, are listed in Table III.

A comparison of the OM calculations carried out with the JLM microscopic OMP and the global phenomenological potential[41] are shown in Figs. 6–8, together with the measured angular distributions. The fits to the data with the phenomenological potential were obtained by a least squares fitting of the strengths of the real and imaginary potentials, V_R and W_D. The ratios between the values of these potentials after searching and their initial values given by the "set A" parametrization in Ref. 41 are called λ_V and λ_W, in analogy with the normalizing parameters described earlier for the microscopic calculations. Table I lists the values of χ^2/N and the normalizing parameters

TABLE III. Neutron global optical model potential below 15 MeV.[a]

Parameters	Set A[a]
V	$54.19-0.33E-\xi(22.7-0.19E)$
W_D	$4.28+0.40E-12.8\xi$
W_V	0.
V_{so}	6.2
r_R	1.198
a_R	0.663
r_I	1.295
a_I	0.59
r_{so}	1.01
a_{so}	0.75

[a]Rapaport *et al.* (Ref. 41); all potential strengths in MeV and geometrical parameters in fm. The quantity ξ is the asymmetry parameter $(N-Z)/A$.

λ_V and λ_W for the phenomenological calculations. The fits to the measured neutron elastic differential cross sections with the phenomenological potential are reasonably good over the whole mass range. This is more or less expected because of the global nature of the parameter set, which was obtained from the simultaneous analysis of neutron elastic scattering from ^{40}Ca, ^{90}Zr, ^{92}Mo, ^{116,124}Sn, and ^{208}Pb in the 7–26 MeV energy range. We note the same difficulties in reproducing the back-angle data on light nuclei as were observed with the microscopic potentials. Somewhat better results can be obtained in light nuclei with phenomenological potentials, but only with geometrical parameters different from those appropriate for medium and heavy nuclei. It is interesting to observe that the microscopic OM calculations, and in particular those carried out with the JLM potential, fit the data equally well and in some cases better than the phenomenological OMP. The lowest values of χ^2/N are obtained with the JLM potential for most of the nuclei listed in Table I.

The variations of the normalizing parameters λ_V and λ_W with A are shown in Table I. Although little normalization is required for the real part of the phenomenological central potential, the imaginary potential must be reduced by a factor whose mean and standard deviation are 0.84 ± 0.10. This is not particularly surprising, as no angular distributions in the energy range between 12 and 20 MeV were included in the determination of the global potential. Moreover, there is a sharp corner (i.e., a discontinuity in the slope) in the energy dependence of the surface imaginary potential at 15 MeV in the potentials of Ref. 41, which is presumably nonphysical.

The total cross sections are shown in Table II. The values calculated with the JLM potential and with the phenomenological model are in reasonable agreement with the experimental values.

V. SUMMARY

In this work, new measurements of neutron angular distributions have been made at 14.6 MeV on targets over a wide mass range (^{9}Be to ^{209}Bi). The data have been com-

pared with optical-model calculations using potentials derived from the microscopic treatments of Brieva and Rook, and of Jeukenne, Lejeune, and Mahaux. They have also been compared with a phenomenological optical model using the geometrical parameters of Rapaport *et al.*[41]

Each of the optical potentials was compared with the data by adjusting the strengths of the real and imaginary parts of the central optical potential. After making these adjustments, it was found that the agreement with the measured angular distributions was reasonable, except at the back angles for the light nuclei (particularly ^{9}Be and C). The required normalizing parameters are within a few percent of unity in all cases for the real potential. The normalizing parameter for the imaginary potential exhibits a mass variation that is most pronounced for the Brieva-Rook potentials. On the other hand, the normalizing parameters for the imaginary parts of the JLM and phenomenological potentials are much closer to constant values (0.96 ± 0.15 and 0.84 ± 0.10, respectively).

The agreement with both the angular distribution data and with measured total cross sections is better for the JLM potentials than for the Brieva-Rook. For the latter, the qualitative discrepancy in fitting the back-hemisphere data in the light nuclei is observed to persist up to roughly $A=60$. The systematic overestimate of the forward-angle cross sections and the total cross sections in the calculations with the Brieva-Rook potentials is consistent with the conclusion of Ref. 49 that these effects are associated with the pronounced deviation of these potentials from a Woods-Saxon shape. It is interesting to point out that our microscopic calculations with the Jeukenne, Lejeune, and Mahaux potential compare quite favorably with calculations using global[40,41] OM potentials, giving in some cases better fits to the data.

ACKNOWLEDGMENTS

We wish to thank Prof. F. Petrovich for continued helpful discussions concerning microscopic optical potentials, and we are indebted to Prof. H. V. von Geramb for suggesting the use of the complex wave number in the exchange approximation. This was performed under the auspices of the U.S. Department of Energy by the Lawrence Livermore National Laboratory under contract number W-7405-ENG-48.

[1]J. R. Smith, Phys. Rev. **95**, 730 (1954).
[2]J. D. Seagrave, Phys. Rev. **97**, 757 (1955).
[3]J. O. Elliot, Phys. Rev. **101**, 684 (1956).
[4]H. Nauta, Nucl. Phys. **2**, 124 (1957).
[5]M. P. Nakada, J. D. Anderson, C. C. Gardner, and C. Wong, Phys. Rev. **110**, 1439 (1958).
[6]J. H. Coon, R. W. Davis, H. E. Felthauser, and D. B. Nicodemus, Phys. Rev. **111**, 250 (1958).
[7]S. Berko, W. D. Whitehead, and B. C. Groseclose, Nucl. Phys. **6**, 210 (1958).
[8]M. M. Khalelskii, Dok. Akad. Nauk. SSSR **113**, 553 (1958).
[9]C. Saint Pierre, M. K. Machwe, and P. Lorrain, Phys. Rev. **115**, 999 (1959).
[10]J. D. Anderson, C. C. Gardner, J. W. McClure, M. P. Nakada, and C. Wong, Phys. Rev. **115**, 1010 (1959).
[11]L. A. Rayburn, Phys. Rev. **116**, 1571 (1959).
[12]W. G. Cross, Nucl. Phys. **15**, 155 (1960).
[13]C. J. Hudson, Jr., W. S. Walker, and S. Berko, Phys. Rev. **128**, 1271 (1962).
[14]C. Wong, J. D. Anderson, and J. W. McClure, Nucl. Phys. **33**, 680 (1962).
[15]C. Deconninck, A. Martegani, J. P. Meulders, and J. Stoquart, Ann. Soc. Sci. Bruxelles **75**, 102 (1961).
[16]B. Ya Guzhovski, At. Energ. **11**, 395 (1961) [Sov. J. At. Energy **11**, 1041 (1962)].
[17]K. Tesch, Nucl. Phys. **37**, 412 (1962).
[18]R. W. Bauer, J. D. Anderson, and L. J. Christensen, Nucl. Phys. **47**, 241 (1963); **48**, 152 (1963); **A93**, 673 (1967).
[19]Yu. V. Dukarevich and A. N. Dyumin, Zh. Eksp. Teor. Fiz. **44**, 130 (1963) [Sov. Phys.—JETP **17**, 89 (1963)].
[20]R. L. Clarke, Nucl. Phys. **53**, 177 (1964).
[21]P. H. Stelson, R. L. Robinson, H. J. Kim, J. Rapaport, and G. R. Satchler, Nucl. Phys. **68**, 97 (1965).
[22]V. S. Nguyen, V. Regis, and R. Boucher, Comptes Rendus **260**, 3922 (1965).
[23]M. Conjeaud, B. Fernandez, S. Harar, J. Picard, and G. Souchere, Nucl. Phys. **62**, 225 (1965).
[24]G. C. Bonazzola, E. Chiavassa, and T. Bressani, Phys. Rev. **140**, 835 (1965); Nucl. Phys. **68**, 369 (1965).
[25]W. J. McDonald, J. M. Robson, and R. Malcolm, Nucl. Phys. **75**, 353 (1966).
[26]A. J. Frasca, R. W. Finlay, R. D. Koshel, and R. L. Cassola, Phys. Rev. **144**, 854 (1966); **156**, 1201 (1967).
[27]C. A. Grin, C. Joseph, J. C. Alder, B. Vaucher, and J. F. Loude, Helv. Phys. Acta **39**, 214 (1966).
[28]R. L. Clarke and W. G. Cross, Nucl. Phys. **A95**, 320 (1967).
[29]D. Spaargaren and C. C. Jonker, Nucl. Phys. **161**, 354 (1971).
[30]M. E. Gurtovoj, A. S. Kukhenko, E. P. Kadkin, B. E. Leschenko, and V. I. Strizhak, At. Energ. **30**, 455 (1971).
[31]P. Kuijper, J. C. Veefkind, and C. C. Jonker, Nucl. Phys. **181**, 545 (1972).
[32]M. Matoba, M. Hyakutake, H. Tawara, K. Tsuji, H. Hasuyama, S. Matsuki, A. Katase, and M. Sonoda, Nucl. Phys. **A204**, 129 (1973).
[33]R. E. Benson, K. Rimawi, E. H. Sexton, and B. Center, Nucl. Phys. **212**, 147 (1973).
[34]W. P. Bucher, C. E. Hollandsworth, and J. E. Youngblood, Phys. Lett. **58B**, 277 (1975).
[35]G. Haouat, J. Lachkar, J. Sigaud, Y. Patin, and F. Coçu, Nucl. Sci. Eng. **65**, 331 (1978).
[36]C. R. Gould, IEEE Trans. Nucl. Sci. **28**, 1264 (1981).
[37]F. Bjorklund and S. Fernbach, Phys. Rev. **109**, 1295 (1958).
[38]F. Perey and B. Buck, Nucl. Phys. **32**, 353 (1962).
[39]D. Wilmore and P. E. Hodgson, Nucl. Phys. **55**, 673 (1964).

[40]F. D. Becchetti, Jr. and G. W. Greenlees, Phys. Rev. **182**, 1190 (1969).
[41]J. Rapaport, V. Kulkarni, and R. W. Finlay, Nucl. Phys. **A330**, 15 (1979).
[42]J. P. Jeukenne, A. Lejeune, and C. Mahaux, Phys. Rev. C **16**, 80 (1977).
[43]A. Lejeune, Phys. Rev. C **21**, 1107 (1980).
[44]F. A. Brieva and J. R. Rook, Nucl. Phys. **A291**, 299 (1977); **A291**, 317 (1977).
[45]H. V. von Geramb, F. A. Brieva, and J. R. Rook, *Lecture Notes in Physics, Vol. 89,* edited by H. V. von Geramb (Springer, Berlin, 1979).
[46]A. Lejeune and P. E. Hodgson, Nucl. Phys. **A292**, 301 (1978).
[47]S. Kailas, S. K. Gupta, M. K. Mehta, and Gulzar Sigh, Phys. Rev. C **26**, 830 (1982).
[48]F. S. Dietrich, R. W. Finlay, S. Mellema, G. Randers-Pehrson, and F. Petrovich, Phys. Rev. Lett. **51**, 1629 (1983).
[49]S. Mellema, R. W. Finlay, F. S. Dietrich, Phys. Rev. C **28**, 2267 (1983).
[50]C. Wong, S. M. Grimes, C. H. Poppe, V. R. Brown, and V. A. Madsen, Phys. Rev. C **26**, 889 (1982). See Refs. 11 and 12 in this paper.
[51]M. Drosg, Nucl. Sci. Eng. **105**, 573 (1972).
[52]S. Mellema (private communication).
[53]G. Bertsch, J. Borysowicz, H. McManus, and W. G. Love, Nucl. Phys. **A284**, 399 (1977).
[54]C. W. Dejager, H. DeVries, and C. DeVries, At. Data Nucl. Data Tables **14**, 479 (1974).
[55]H. Fiedeldey, Nucl. Phys. **77**, 149 (1966).
[56]D. G. Foster, Jr. and D. W. Glasgow, Phys. Rev. C **3**, 576 (1971).
[57]Ch. Lagrange and A. Lejeune, Phys. Rev. C **25**, 2278 (1982).
[58]Ch. Lagrange and J. C. Brient, J. Phys. (Paris) **44**, 27 (1983).
[59]D. J. Stubeda, M. LeMere, and Y. C. Tang, Phys. Rev. C **17**, 447 (1978).
[60]A. S. Meigooni, J. S. Petler, and R. W. Finlay, Phys. Med. Biol. **29**, 643 (1984).
[61]F. Petrovich (private communication).